Irregular variations in the melting point of size-selected atomic clusters

Martin Schmidt, Robert Kusche, Bernd von Issendorff & Hellmut Haberland

Fakultät für Physik, Universität Freiburg, H. Herderstrasse 3, D-79104 Freiburg, Germany

Small particles have a lower melting point than bulk material[1]. The physical cause lies in the fact that small particles have a higher proportion of surface atoms than larger particles—surface atoms have fewer nearest neighbours and are thus more weakly bound and less constrained in their thermal motion[2,3] than atoms in the body of a material. The reduction in the melting point has been studied extensively for small particles or clusters on supporting surfaces. One typically observes a linear reduction of the melting point as a function of the inverse cluster radius[2,4,5]. Recently, the melting point of a very small cluster, containing exactly 139 atoms, has been measured in a vacuum using a technique in which the cluster acts as its own nanometre-scale calorimeter[6,7]. Here we use the same technique to study ionized sodium clusters containing 70 to 200 atoms. The melting points of these clusters are on average 33% (120 K) lower than the bulk material; furthermore, we observe surprisingly large variations in the melting point (of ±30 K) with changing cluster size, rather than any gradual trend. These variations cannot yet be fully explained theoretically.

The melting point (T_{melt}) of small particles is not only of scientific interest, but also has some technological implications. In sintering processes, fine powders are compressed and heated until they coalesce. If extremely fine powders are employed, a lower sintering temperature could be used. Also, the present drive towards nanoscale technology leads to smaller and smaller geometric dimensions with a concomitant reduction of T_{melt} and consequently reduced electrical and mechanical stability at elevated temperatures.

The standard way to measure T_{melt} of a material is to heat it and record the temperature at which it becomes liquid. In order to do this, one needs some physical property which changes measurably at T_{melt}. For example, the electron-diffraction pattern of a crystalline solid, which vanishes on melting, has been used to study the melting of small particles supported on surfaces[4,5] or in cluster beams[8]. In both cases one has to work with broad size distributions. Moreover, in the case of the surface experiments the physical properties of the clusters could be affected by the surface contact. There exist two earlier experiments on the melting of free, size-selected clusters: one studied the temperature dependence of the ionization energy of sodium clusters[9], the other looked for a transition of methanol hexamers[10].

A deeper insight into the solid-to-liquid phase transition may be gained by measuring the relation between temperature and internal energy across the melting point. For a macroscopic material this is achieved by placing the sample in a thermally insulated box, containing an electric heater and a thermometer. Some known amount of energy U is supplied to the material by heating, and its temperature T is measured. The relation between temperature and energy, $U = U(T)$, is called the caloric curve, its derivative is the heat capacity $c(T) = \partial U/\partial T$, and the equipment used to measure it is called a calorimeter. At the melting point, there is a step in the caloric curve (as shown in Fig. 2), which is simple to understand. We

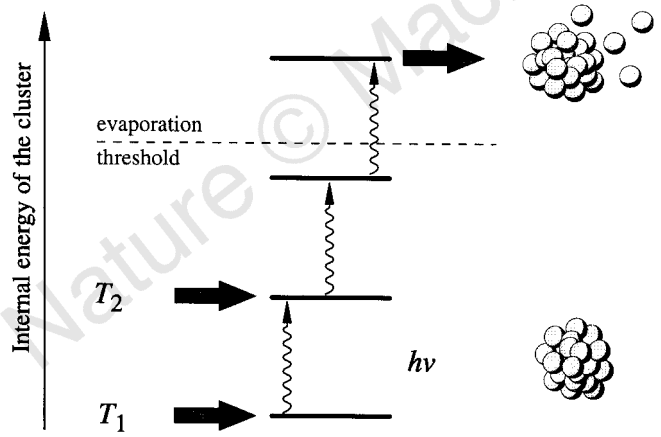

Figure 1 The basic idea of the experiment is to heat a cluster at temperature T_1 by absorbing a photon of energy $\delta U = h\nu$. The increased temperature of the cluster, T_2, is then identified by increasing the cluster source temperature until the thermally heated clusters show the same photofragmentation behaviour as the laser-heated ones. This procedure can be divided into four steps. (1) A mass-selected beam of cluster ions of temperature T_1 is prepared in vacuum. (2) The clusters are irradiated by photons from a laser. The photon energy ($h\nu = 3.1\,\text{eV} \approx 10^{-18}\,\text{J}$) quickly relaxes into vibrations and heats the cluster to a temperature T_2, where the clusters do not emit atoms on the 100-μs timescale of the experiment. Only the absorption of more photons from the same laser pulse (two are shown here) raises the temperature above T_{evap}, the temperature needed for evaporation of atoms from the cluster. (3) The size distribution of the remaining cluster ions is measured, which is a very sensitive measure of the cluster's internal energy. (4) The cluster temperature is now raised to T_2 where the absorption of only two photons leads to the *same* number of evaporated atoms. An energy increase δU thus leads to a temperature increase $\delta T = T_2 - T_1$. For small enough δT, the ratio $\delta U/\delta T$ equals the heat capacity $c(T)$. In our experiment this is the case, as discussed in more detail in ref. 6.

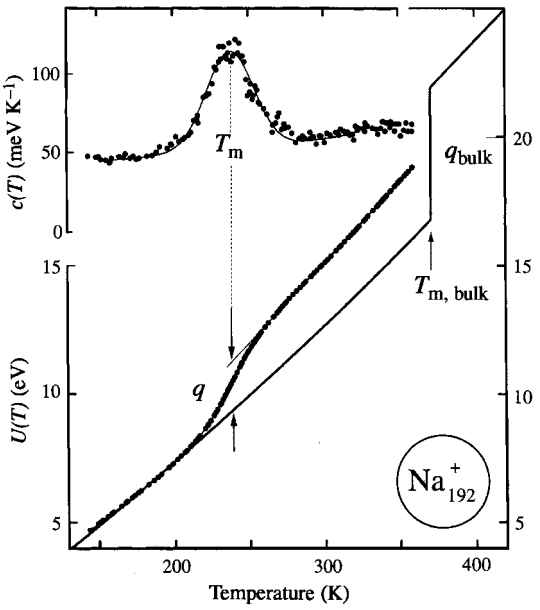

Figure 2 Heat capacity $c(T)$ and its integral, the caloric curve $U(T)$, for a positively charged sodium cluster containing exactly 192 atoms. The solid dots show the experimental results. From the maximum of $c(T)$ one obtains the melting point T_{melt}, and from the height of the smoothed-out step in the caloric curve one gets the latent heat of fusion q, that is, the energy necessary to destroy the crystalline lattice at the melting point. The thick solid line is the bulk caloric curve scaled to 192 atoms. $T_{m,bulk}$ and q_{bulk} are the bulk melting point and latent heat of fusion, respectively. Heat-capacity curves have been measured for sodium clusters with 70–200 atoms. Melting points and latent heats have been extracted and are shown in Fig. 3b and c.

consider a piece of ice floating in water, in thermal equilibrium at a temperature of 0 °C. Heating this system with a small amount of energy would not lead to a temperature increase: instead, the energy would be used to melt the ice. Hence the energy increases without a temperature increase, which corresponds to a vertical line in the caloric curve. The height of the step is equal to the energy needed to destroy the crystalline lattice at T_{melt}. This energy is called the latent heat of fusion q.

A large sample mass is required for such a calorimeter in order to minimize the effects of the thermal capacities of the heater and thermometer. The limit of the technologically possible is reached when the heater and thermometer are the same supporting microstructure. This has been achieved recently in an experiment on supported tin clusters[5].

The ultimate miniaturization of the calorimeter is reached if one dispenses entirely with supporting surface, heater and thermometer. It was shown earlier[6,7] that this is indeed possible, by measuring the internal energy of free clusters with a variable temperature. Clusters can be thermalized by embedding them for some time in an inert buffer gas of known temperature[6,9,11]. To measure their internal energy, known amounts of energy are added by irradiating the clusters with a laser. By counting the number of evaporated atoms one can determine the internal energy of the cluster before the irradiation. Such a procedure, however, still requires input parameters like the atom binding energies, which are not known accurately enough. We have instead used a differential measuring scheme, which does not require any parameters except for the photon energy and the temperature of the clusters before they absorb a photon. This is explained in Fig. 1 and in more detail in refs 6 and 7.

One example of a caloric curve that we obtained in this way is given in Fig. 2. The caloric curves of small particles do not have a sharp step at T_{melt}, but show a more gradual increase. The finite width of the step is due to the finite number of atoms in the cluster[2–4]; only in the limit of very many atoms does the increase become step-like. We measured caloric curves for sodium clusters containing between 70 and 200 atoms. The corresponding melting points and latent heats are given in Fig. 3b and c. Neither value shows the expected gradual increase to the bulk value, but rather shows a pronounced structure, which to our knowledge has not been experimentally observed before. Changing the cluster size by just one atom can shift the melting point by several degrees.

Similar variations of the melting point have been predicted in a theoretical treatment of argon clusters[12]. Argon clusters are very simple systems, in which the atoms tend to organize in onion-like shells of icosahedral symmetry. Completion of shells occurs at cluster sizes $N = 13, 55, 147, 309 \ldots$; for these "magic numbers" local maxima of T_{melt} were found, which can be explained by the enhanced rigidity of argon clusters with completed shells.

The question arises whether such a simple argument is appropriate also for the observed behaviour of our sodium cluster melting points. Depending on size, the stability of sodium clusters can be explained using two different concepts: electronic and geometric shell closings[9,13,14]. Sodium clusters are surprisingly well described by the 'nearly free electron model', in which the valence electrons are treated as nearly free, being caged only by the cluster's surface[13,14]. The electrons are grouped in shells (similar to what is known for atoms or nuclei), and on closing such a shell, the electronic contribution to the binding energy of an atom reaches a maximum[13,14]. This is demonstrated by the mass spectrum of hot sodium clusters shown in Fig. 3a. The maxima (magic numbers) correspond to clusters with closed electronic shells. They have a larger binding energy, and are thus more resistant to evaporation.

Could an increased binding energy per atom lead to an increased melting point? The mass spectrum shows the stability with respect to evaporation, where an atom and its valence electron leave the cluster. The loss of one electron requires a lot of energy for a closed-shell cluster, which therefore has a high binding energy. On melting, conversely, the number of valence electrons stays the same. One can thus expect that electronic shells should be more visible in the fragmentation pattern than in the melting process. Nevertheless, there are some similarities. There is a maximum near Na_{93}^{+} in both cases. Also, near 139 atoms, where there is the next electronic shell closing, there is a maximum in T_{melt}. However, a more detailed examination of this size region showed that the peak of T_{melt} occurs at 142 atoms, where the intensity of the mass spectrum (and thus the binding energy of the clusters) has already decreased. The differences become more marked at the next electronic shell closing near 197 atoms, where there are no special features in the melting point. The effects of the shell closing on the size dependence of the latent heat q are even less marked. The electronic structure of the clusters

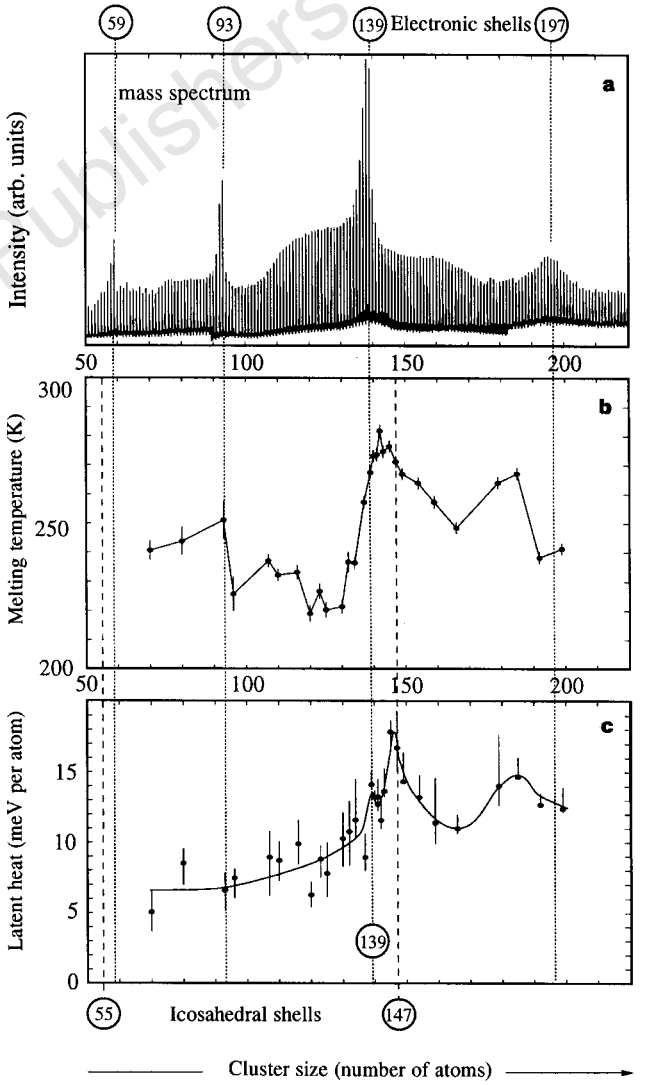

Figure 3 Three different data sets plotted against the cluster size. **a**, Mass spectrum of hot, positively charged sodium clusters ($T \approx 400$ K). The enhanced intensities of the so-called "magic" cluster sizes can be explained by higher dissociation energies at the electronic shell-closings[13,14] indicated above the figure. These numbers (59, 93, …) correspond to the number of atoms in the cluster. One obtains the number of valence electrons by subtracting one unit. **b**, Melting-point temperatures. The values change strongly with cluster size and show some weak correlation with electronic shell closings. The sodium bulk value (371 K) is far above the cluster melting points. **c**, Latent heat of fusion. The bulk value is 27 meV per atom. The number of atoms where icosahedral shell closings[9] occur are indicated below the figure.

can thus explain the magic numbers of the mass spectrum, but not the size-dependence of T_{melt} and q.

For large sodium clusters of several thousand atoms, geometrical shell closings can explain the intensities in a mass spectrum[9]. But smaller clusters could also have an icosahedral structure, and although this does not show up in the mass spectrum, it might well have an influence on the cluster melting points. There is an icosahedral shell closing at 147 atoms, and indeed the latent heat has a pronounced maximum in this region. However, it is not possible to explain all the observed features by geometrical models, either by the icosahedral structure mentioned above, or by the modified pentagonal bipyramid structures favoured by gold clusters in this size range[15]. Thus geometrical shell closing arguments cannot explain the size dependence of either T_{melt} or q.

We therefore conclude that the size dependence of melting-point temperature and latent heat of fusion cannot be explained by one simple argument. There is probably a complicated interplay between geometric and electronic structure, presenting a challenge for theory. □

Received 8 December 1997; accepted 16 February 1998.

1. Pawlow, P. Über die Abhängigkeit des Schmelzpunktes von der Oberflächenenergie eines festen Körpers. *Z. Phys. Chem.* **65,** 1–35 (1909).
2. Couchman, R. R. The Lindemann hypothesis and the size dependence of melting temperatures II. *Phil. Mag. A* **40,** 637–643 (1979).
3. Berry, R. S. When the melting and freezing point are not the same. *Sci. Am.* **263,** 50–56 August (1990).
4. Buffat, Ph. & Borel, J. P. Size effect on the melting temperature of gold clusters. *Phys. Rev. A* **13,** 2287–2298 (1976).
5. Lai, S. L., Guo, J. Y., Petrova, V., Ramanath, G. & Allen, L. H. Size-dependent melting properties of small tin particles: nonocalorimetric measurements. *Phys. Rev. Lett.* **77,** 99–102 (1996).
6. Schmidt, M., Kusche, R., Kronmüller, W., v. Issendorff, B. & Haberland, H. Experimental determination of the melting point and heat capacity for a free cluster of 139 sodium atoms. *Phys. Rev. Lett.* **79,** 99–102 (1997).
7. Bertsch, G. Melting in clusters. *Science* **277,** 1619 (1997).
8. Hovick, J. W. & Bartell, L. S. Phase and phase-changes in tert-butyl thiol. *J. Mol. Struct.* **413,** 615–620 (1997).
9. Martin, T. P. Shells of atoms. *Phys. Rep.* **273,** 199–241 (1996).
10. Buck, U. & Ettischer, I. Experimental evidence for an isomeric transition of size selected methanol hexamers. *J. Chem. Phys.* **100,** 6974–6976 (1994).
11. Ellert, Ch., Schmidt, M., Schmitt, Ch., Reiners, Th. & Haberland, H. Temperature dependence of the optical response of small, open shell sodium clusters. *Phys. Rev. Lett.* **75,** 1731–1734 (1995).
12. Wales, D. J. & Berry, R. S. Freezing, melting, spinodals, and clusters. *J. Chem. Phys.* **92,** 4473–4481 (1990).
13. de Heer, W. A. The physics of simple metal clusters: experimental aspects and simple models. *Rev. Mod. Phys.* **65,** 611–676 (1993).
14. Brack, M. The physics of simple metal clusters: self-consistent jellium model and semi-classical approaches. *Rev. Mod. Phys.* **65,** 677–732 (1993).
15. Cleveland, C. L. *et al.* Structural evolution of smaller gold nanocrystals: the truncated decahedral motif. *Phys. Rev. Lett.* **79,** 1873–1876 (1997).

Acknowledgements. This work was supported by the Deutsche Forschungsgemeinschaft.

Correspondence and requests for materials should be addressed to H.H. (e-mail: hellmut@frha06.physik.uni-freiburg.de).

Carbon nanotubes as long ballistic conductors

C. T. White*† & T. N. Todorov*

** Department of Materials, University of Oxford, Parks Road, Oxford OX1 3PH, UK*

Early theoretical work on single-walled carbon nanotubes[1–3] predicted that a special achiral subset of these structures known as armchair nanotubes[3] should be metallic. Tans *et al.*[4] have recently confirmed these predictions experimentally and also showed directly that coherent electron transport can be maintained through these nanowires up to distances of at least 140 nm. But single-walled armchair nanotubes are one-dimensional conductors with only two open conduction channels (energy subbands in a laterally confined system that cross the Fermi level)[1–3]. Hence, with increasing length, their conduction electrons ultimately become localized[5] owing to residual disorder in the tube which is inevitably produced by interactions between the tube and its environment. We present here calculations which show, however, that unlike normal metallic wires, conduction electrons in armchair nanotubes experience an effective disorder averaged over the tube's circumference, leading to electron mean free paths that increase with nanotube diameter. This increase should result in exceptional ballistic transport properties and localization lengths of 10 μm or more for tubes with the diameters that are typically produced experimentally[6].

Once physisorbed on a surface, even an initially perfect metallic carbon nanotube is disordered because of residual interactions with the substrate. In general, for such long thin conductors at zero temperature, the theory of transport through weakly disordered materials predicts a transition to a localized regime (where the resistance R is exponentially large) around a wire length where R reaches a value of one quantum resistance unit[7], $r = h/2e^2$. Deep within the localized regime the resistance increases exponentially with length L as $R(L) \sim e^{L/\xi}$, where ξ is the localization length for electrons in the disordered wire[8]. For wires with N_C open conduction channels, ξ is given within a factor of order unity by $\xi = N_C l$ (refs 9, 10) where l is the elastic mean free path for backward electron scattering. Hence for wires with $N_C \gg 1$, the motion of the electron on the scale of ξ is largely diffusive, but for weakly disordered, small-diameter armchair nanotubes, which have $N_C = 2$, this motion is largely ballistic. This analysis suggests immediately that any observable quantum transport through these nanotubes is also ballistic.

For a fixed amount of disorder, as the transverse size of a normal metallic quantum wire increases l remains largely fixed but ξ increases due to the introduction of new channels at the Fermi level, ϵ_F (see ref. 10 and refs therein). However, this behaviour does not lead to long localization lengths in armchair carbon nanotubes because N_C remains pinned at two. We will show, however, that for a fixed amount of disorder as the radius of a small-diameter armchair tube increases, l does not remain fixed but rather increases leading to long localization lengths. We will also show that this remarkable behaviour arises because of the special character of the armchair states close to ϵ_F in the perfect tube and hence does not depend crucially on the details of the disorder.

To study the effects of disorder on the transport properties of armchair nanotubes we adopt the usual tight-binding model which retains only the nearest neighbour π-like hamiltonian matrix elements between $|p_\perp\rangle$ orbitals (one per carbon atom) orientated normal to the tubule surface[1,3]. Local density-functional calculations have established that this model, with all diagonal matrix elements fixed at ϵ_F and all non-zero off-diagonal matrix elements fixed at $V_0 = -2.7$ eV provides an excellent description of the valence bands of perfect armchair carbon nanotubes in the vicinity of ϵ_F (refs 1, 11). The effects of disorder can then be incorporated into the model (referred to here as the 'full model') by assuming that these diagonal and off-diagonal matrix elements are not fixed at their values in the perfect tube but are independent random variables with variances σ_ϵ^2 and σ_V^2, respectively.

In the absence of disorder, the full model yields $2N_B$ bands as a function of the quasi-momentum k that labels an eigenstate of the helical screw operator $S(\theta_0, z_0)$ used to generate the $[N_B, N_B]$ armchair tube by starting with a single ring, such as highlighted in Fig. 1a, and then rotating this ring by $\theta_0 = \pi/N_B$ radians around the tubule axis followed by a translation $z_0 = (\sqrt{3}/2)d_0$ along this axis[11]. Each ring contains $2N_B$ carbon atoms and has a radius $r_T = (3d_0/2\pi)N_B$, where N_B is the number of C–C bonds in the ring and $d_0 = 0.142$ nm is the C–C bond distance. The a_1 and a_2 bands that cross at $k_F = 2\pi/3$ are present in all armchair tubules[1]. These two bands are highlighted in Fig. 1b for the [10,10] tube. In the absence of disorder, symmetry can be used to block diagonalize the full model to the point that the a_1 and a_2 bands are described

† Permanent address: Code 6179, Naval Research Laboratory, Washington DC 20375, USA.